View metadata, citation and similar papers at core.ac.uk
brought to you by CORE
provided by CERN Document Server

CERN-LHCC-2007-028
LHCC-RD-014
RD Status Report/RD39
21st November 2007

RD39 STATUS REPORT 2007

CERN RD39 Collaboration

X.Rouby[j], P. Anbinderis[m], T. Anbinderis[m], N. D'Ambrosio[k], R. Bates[e], W. de Boer[h], E. Borchi[c], M. Bruzzi[c], S. Buontempo[k], C. Buttar[e], W. Chen[b], V. Cindro[i], V. Eremin[l], A. Furgeri[h], E. Gaubas[m], E. Grigoriev[d], J. Härkönen[g], E. Heijne[a], I. Ilyashenko[l], V. Kalesinskas[m], M. Krause[h], Z. Li[b], P. Luukka[g], I. Mandic[i], D. Menichelli[c], M. Mikuz[i], O. Militaru[j], S. Mueller[h], T.O. Niinikoski[a], V. O'Shea[e], S. Pagano[k], C. Parkes[e], K. Piotrzkowski[j], S. Pirollo[c], P. Pusa[f] J. Räisänen[f], E. Tuominen[g], E. Tuovinen[g], J. Vaitkus[m], E. Verbitskaya[l], S. Väyrynen[f], M. Zavrtanik[i]

[a]*CERN, CH-1211 Geneva, Switzerland*
[b]*Brookhaven National Laboratory, Upton, NY 11973-5000, USA*
[c]*Dipartimento di Energetica, Universitá di Firenze, I-50139 Firenze, Italy*
[d]*Department de radiologie, Université de Geneve, CH-1211 Geneve, Switherland*
[e]*Department of Physics and Astronomy, University of Glasgow, Glasgow G12 8QQ, United Kingdom*
[f]*Accelerator Laboratory, University of Helsinki, 00014 University of Helsinki, Finland*
[g]*Helsinki Institute of Physics, 00014 University of Helsinki, Finland*
[h]*IEKP University of Karlsruhe, D-76128 Karlsruhe, Germany*
[i]*Jozef Stefan Institute, Experimental Particle Physics Department, 1001 Ljubljana, Slovenia*
[j]*Université Catholique de Louvain, FYNU, Louvain-la-Neuve, Belgique*
[k]*Dipartimento di Fisica, Università degli Studi di Salerno and INFN, I-84081 Baronissi (SA), Italy*
[l]*Ioffe Physico-Technical Institute, Russian Academy of Sciences, St.Petersburg 194021, Russia*
[m]*University of Vilnius, Institute of Materials Science and Applied Research, 2040 Vilnius, Lithuania*

Summary

CERN RD39 Collaboration is aiming for development of super-radiation hard cryogenic silicon detectors for applications of LHC experiments and their future upgrades. Radiation hardness up to 1×10^{16} n_{eq}/cm^2 is required in the future HEP experiments. The most important measure of the detector's radiation hardness is the Charge Collection Efficiency (CCE), which is affected by both the detector sensitive volume (depletion depth) and charge trapping by radiation-induced trapping centers. However, 1×10^{16} n_{eq}/cm^2 fluence is well beyond the radiation tolerance of even the most advanced semiconductor detectors fabricated by commonly adopted technologies. First, the full depletion voltage (V_{fd}) will be in the thousands of volts for a 300 μm thick Si detector operated at or near room temperature. Second, the charge carrier trapping will limit the charge collection depth to an effective range of 20 μm to 30 μm regardless of depletion depth. In order to maintain an acceptable CCE under Super LHC radiation environment, one has to solve both problems simultaneously.

The CERN RD39 Collaboration has launched in 2005 a project to build Transient Current Technique (TCT) and Charge Collection Efficiency (CCE) set-ups at CERN with temperature range from 35 K to 300 K (C-TCT). The C-TCT project was successfully completed in 2006. From TCT data it is possible to extract the full depletion voltage, effective trapping time, electric field distribution and the sign of the space charge in the silicon bulk. The interest in the extension of the temperature range down to helium temperatures is not only in the Super LHC tracker detectors, but also in the basic understanding of heavily radiation-damaged silicon. Our first results show that the trapping time constant increases and the V_{fd} decreases at the temperatures below 200K.

We have developed the advanced radiation hard detectors using charge or current injection, the current injected detectors (CID). In a CID, the electric field is controlled by injected current, which is limited by the space charge. This leads to nearly uniform electric field through the detector at any operating voltage regardless of the radiation fluence. The charge collected in 300 μm thick CID at 1×10^{16} n_{eq}/cm^2 is estimated to be equivalent of 5000 electrons at the 500V bias. This is more than in a standard detector hypothetically fully depleted with thousands of volts. The elevated CCE is observed already at 220K. An important advantage of CID is that at some given operating voltage, the current decreases with increasing irradiation fluence. This would result in segmented detector decreasing shot noise with respect of increasing fluence. With CID concept it is additionally possible to increase the absolute value of the colleted charge when the concentration of active trapping centers is reduced by cooling to low temperatures. The CID's current-voltage and CCE properties have been confirmed in 2006 by many independent measurements.

1. Introduction

For silicon detector applications in current high energy physics experiments, such as those in Large Hadron Collider (LHC) at CERN, the main effort has been directed so far towards the improvement (or reduction) of the detector full depletion voltage [1], which leads to the increase of detector sensitive volume and therefore the detector charge collection efficiency (CCE). This remains true if the level of radiation environment is in the order of 1×10^{15} n_{eq}/cm^2.(n_{eq} is the 1 MeV neutron equivalent fluence) , when the trapping of carriers by radiation-induced defects are not significant (< 50%). However, for LHC upgrade, the Super-LHC (SLHC), the expected radiation level will be 10 time higher, up to 1×10^{16} n_{eq}/cm^2. In this case, in addition to the detector full depletion problem, the trapping problem is not one of the main limiting factors to CCE.
The total charge collected by a detector, Q, can be considered to be a product of two terms [2]:

$$Q = Q_0 \cdot CCE_{GF} \cdot CCE_t \equiv Q_0 \cdot \vartheta \cdot \eta \tag{1}$$

The term $CCE_{GF} = \vartheta$ in Eq. (1) is the geometrical factor, that is related to the detector depletion thickness w, the waiting function (detector segmentation scheme) [3-4], and the detector configuration (e.g. planar detectors or 3d detector) [5]. The term $CCE_t \equiv \eta$ is the trapping factor. For a simple planar pad detector with no segmentation, the weighting field E_w is $1/d$ [3], and the induced current by a moving charge $Q_0^{'}(t)$ is [6]:

$$i(t) = Q_0^{'}(t) \cdot E_w \cdot V_{dr}(t) = Q_0^{'}(t) \cdot \frac{1}{d} \cdot V_{dr}(t) \tag{2}$$

where $V_{dr}(t)$ is the carrier drift velocity that depends on the detector internal electric field, and $Q_0^{'}(t)$ is affected by trapping (for large detrapping constant) [6]:

$$Q_0^{'}(t) = Q_0 \cdot e^{-t/\tau_t} \tag{3}$$

Where τ_t is the trapping time constant that is proportional inversely to the trap concentration, and the total collected charge in Eq. (1) can be rewritten as, using Eq. (2) and (3):

$$Q = \int_0^{t_{dr}} i(t)dt = \int_0^{t_{dr}} Q_0 \cdot e^{-t/\tau_t} \cdot \frac{1}{d} \cdot V_{dr}(t)dt \tag{4}$$

Where t_{dr} is the carrier transient time or drift time. For simplicity, we assume a constant electric field and therefore constant carrier drift velocity V_{dr}, we have:

$$Q = Q_0 \cdot \frac{w}{d} \cdot \frac{\tau_t}{t_{dr}}(1 - e^{-t_{dr}/\tau_t}), \text{ with } \theta = \frac{w}{d} \text{ and } \eta = \frac{\tau_t}{t_{dr}}(1 - e^{-t_{dr}/\tau_t}) \tag{5}$$

where w is the detector full depletion, and the expression $w = V_{dr} \cdot t_{dr}$ is used. The overall $CCE = Q/Q_0 = \vartheta \cdot \eta$ is plotted in Fig. 1.

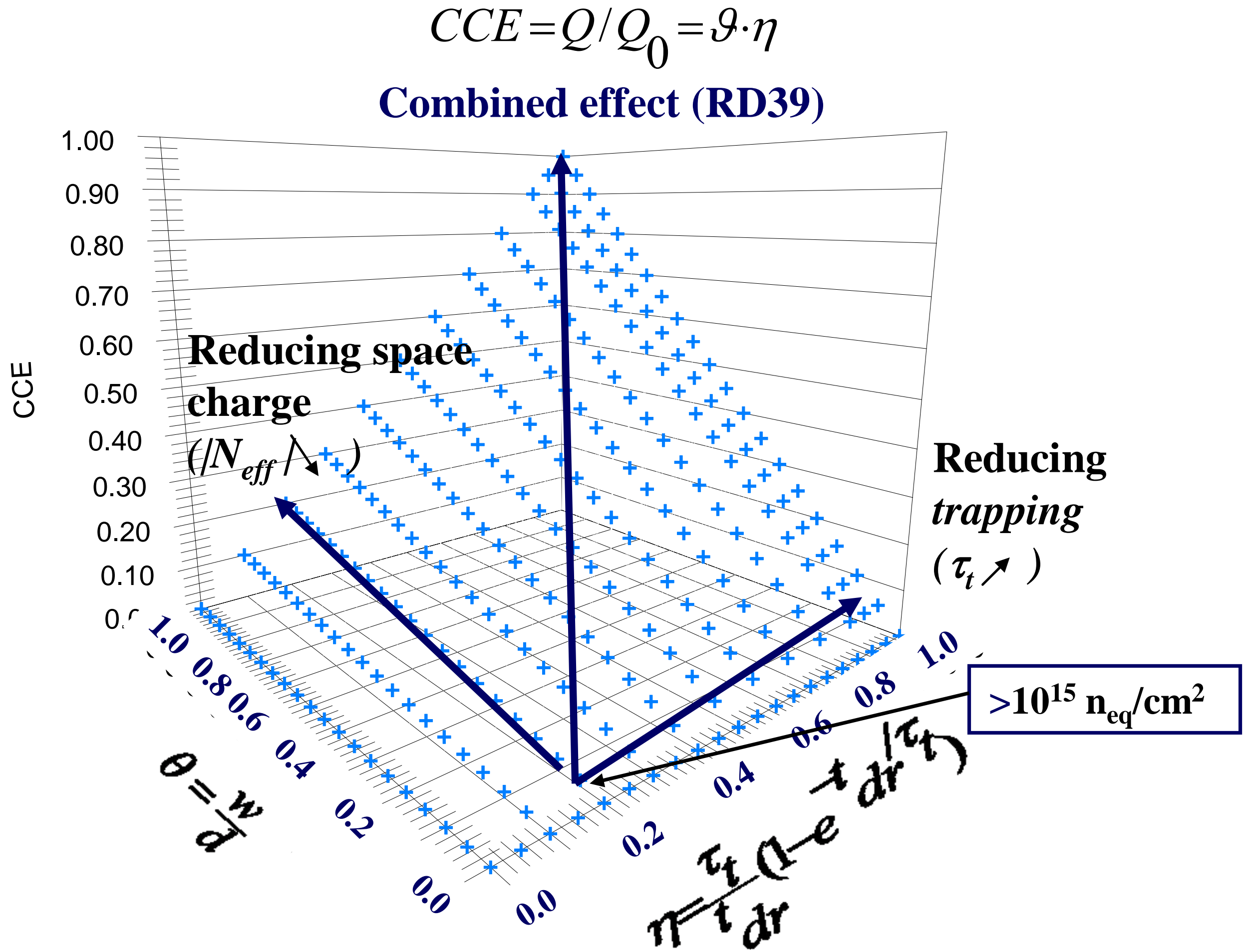

Figure 1. Illustration of influence of space charge and trapping on total Charge Collection Efficiency (CCE).

If Q_0 is the total charge deposited by a Minimum Ionizing Particle (MIP) particle in a detector of the thickness of d, then it can be expressed in terms of the number of electrons as the following:

$$Q_0 = 80 \cdot d \quad \text{(Electrons, here } d \text{ is in } \mu\text{m)} \tag{6}$$

and Eq. (5) can be rewritten as:

$$Q = 80w \cdot \frac{\tau_t}{t_{dr}}(1 - e^{-t_{dr}/\tau_t}) \quad \text{(Electrons, here } w \text{ is in } \mu\text{m)} \tag{7}$$

For situation with large trapping, such as in the SLHC with up to 10^{16} n_{eq}/cm^2 radiation, $\frac{\tau_t}{t_{dr}} << 1$, we have:

$$Q \cong 80w \cdot \frac{\tau_t}{t_{dr}} = 80 \cdot V_{dr} \cdot \tau_t \equiv 80 \cdot d_{CCE} \quad \text{(Electrons)} \qquad \text{(very high fluences, } \frac{\tau_t}{t_{dr}} << 1\text{)} \tag{8}$$

where $d_{CCE} = V_{dr} \cdot \tau_t$ is defined as the charge collection distance and it is in the order of 20 μm for 10^{16} n_{eq}/cm^2 radiation if one uses the trapping time constant of about 0.2 ns, and saturation drift velocity of 10^7 cm/s [7] . It is clear that at very high fluences, the collected charge depends only on the charge collection distance that is usually much less than the detector thickness. In this case, it does not matter if a detector with thickness of $d \geq 50$ μm is fully depleted or not, the collected charge is about the same if $w \geq d_{CCE}$, and it is in the order of 1600 e's for 10^{16} n_{eq}/cm^2 radiation, regardless of the detector thickness ($d \geq d_{CCE}$).

For low or modest radiation fluences, where $\frac{\tau_t}{t_{dr}} >> 1$, Eq. (7) can be re-written as:

$$Q = 80w \cdot \left(1 - \frac{1}{2} \cdot \frac{t_{dr}}{\tau_t}\right) \quad \text{(Electrons)} \qquad \text{(low or modest fluences, } \frac{\tau_t}{t_{dr}} >> 1\text{)} \tag{9}$$

In this case, the detector depletion depth w is still an important factor in the collected charge, which depends on the bias voltage:

$$w = \sqrt{\frac{2\varepsilon\varepsilon_0 V}{eN_{eff}}} \tag{10}$$

where e is the electronic charge, ε the permittivity of Si, ε_0 the permittivity of vacuum, V the bias voltage, and N_{eff} the effective space charge density.
Obviously, to increase CCE, one has to increase CCE_G and CCE_t simultaneously, as shown in Fig. 1.

The trapping (τ_t) and detrapping (τ_d) time constants for a trap level can be defined by:

$$\begin{cases} \tau_t = \dfrac{1}{\sigma v_{th} N_t} \\ \tau_d = \dfrac{1}{\sigma v_{th} N_C e^{-E_t/kT}} \end{cases} \tag{11}$$

where σ is the capture cross section of the trap, v_{th} is the thermal velocity of charge carriers, N_T is the concentration of traps, N_C the electric state density in the conduction band, and E_t the trap energy level in the band gap.
The trapping time constant is nearly independent on temperature (or weak dependence on T). However, it depends strongly on the radiation fluence Φ_n. At a fluence of 10^{16} n_{eq} $/cm^2$, the trapping time can be as short as 0.2 ns [7]. We can again estimate the trapping effect from different respect. Due to the saturation of carrier drift velocity at about 10^7 cm/s value, the maximum distance of charge drift before being trapped is about t = 20 μm (if $t < w$). This will cause an induced charge of $Q(t) = Q(w) \cdot t/w$, where $Q(w)$ is charges generated in the depletion region $Q(w) = Q_0 \cdot w/d$ (Q_0 is the total charge generated in the detector). Therefore the total induced charge in a detector with thickness d, a

depletion depth w, and a trapping distance t is $Q = Q(t) = Q_0 \cdot t/d$. We note here that this charge has no explicit dependence on depletion depth w, except that $w > t$. In fact this charge is the same as that of a fully depleted detector with a thickness t: $Q = Q(t) = Q_0(t) \cdot t/t = Q_0(t)$. But since $Q_0(t) = Q_0(d) \cdot t/d = Q_0 \cdot t/d$, we have, for this detector with a thickness of t, that $Q = Q(t) = Q_0 \cdot t/d$, which is the same as before. Therefore the effective detector thickness for CCE is the trapping distance. Note here that the trapping distance t here is the same as the charge collection distance d_{CCE} defined before in Eq (8). Thus At a fluence of 10^{16} n_{eq} /cm^2, >90% detectors volume (for a typical thickness of 200-300 μm) would represent an effective dead space. The estimation done above again is for a pad detector with no segmentation, and a simple weighting field. For a real segmented detector with complicated weighting field, the charges might not be the same, but they should be in the same order of magnitude.

As demonstrated by the previous RD39 results [8], the CCE_{GF} can be increased close to 1 by manipulating the electric field in the detector via current and/or charge injection at temperatures from 130 K to 150 K. Since for fluence less than 1×10^{15} n_{eq}/cm^2, the trapping term CCE_t is less significant, CCE can be significantly improved by improving only the CCE_{GF} at temperatures from 130 K to 150 K. However, for extremely high fluence (10^{16} n/cm^2) in LHC upgrade environment, the trapping term can also be significant and affect the CCE greatly. The approach of RD39 to overcome the fundamental trapping problem at very high fluencies is to modify the CCE_t at the low temperatures. The key of our approach is to use CID (current injected detector) mode to modify the detector electric field profile such that the detector is virtually fully depleted at any fluences, and to fill the traps to increase the trapping time constant that affects charge collection efficiency (CCE). Temperatures in the range of 220 to 250 K may be possible for CID operation.

2. Cryogenic Transient Current Technique (C-TCT) project

The CERN RD39 Collaboration has constructed Transient Current Technique (TCT) measurement setup, which is capable to operate below liquid nitrogen temperatures. By analyzing the current transients, it is possible to extract the full depletion voltage, effective trapping time, electric field distribution and the sign of the space charge in the silicon bulk. Our results show that the effective space charge and trapping can be manipulated by charge injection and temperature. This might allow significantly higher Charge Collection Efficiency (CCE) compared to the detectors operating under normal reverse bias and at temperatures from 0° to -30° C.

The TCT measurement is based on the detection of the dominant type of charge carrier, electron or hole, which drifts across the whole detector thickness after being excited by a photon. This is achieved by illuminating (i.e. a $n^+/p^-/p^+$ device) the front (n^+ implant) or back (p^+ implant) side of the detector with a red laser, whose light creates electron-hole pairs close to the device surface. When the front-side of the detector is illuminated, the electrons move only a few microns (small signal) and are gathered to the n^+-electrode so fast that the signal is damped by the rise-time of the data acquisition

electronics and therefore the measured signal is mainly coming from the holes that travel a longer distance through the silicon bulk. Correspondingly, when a $p^+/n^-/n^+$ detectors front side is illuminated, mainly the electron current is measured. By analyzing the transient, it is possible to extract the full depletion voltage, effective trapping time, electric field distribution and the sign of the space charge in the silicon bulk.

Our TCT setup consists of LeCroy 3 GHz bandwidth oscilloscope, Keithley 6487 source meter unit capable to source up to 500V, vacuum chamber, cold finger, Leybold helium stirling cooler, temperature and vacuum control units. The detectors signal is transferred by coaxial RF transmission line specially designed for cryogenic applications [5]. The measurements are recorded by LabView based data acquisition system. The system has two lasers emitting 678 and 1060 nm light. As mentioned above, the measurement with red laser provides information about the space charge, while the infrared (IR) laser illumination generates electron hole pairs homogenously through the entire silicon bulk. Thus, the transient recorded from the IR laser measurements consist of electron and hole currents both and simulate minimum ionizing particles (MIP) [9]. The lasers and its driver are supplied by the Advanced Laser Diode Systems A.L.S. GmbH. The width of the laser pulse is about 30 ps (FWHM) and the maximum optical power is 250 mW. The lasers can be tuned ranging 0-100%. The trigger rate can be adjusted from 1 MHz to single shots. During the measurements, the lasers are operated typically at 10-50 Hz repetition rate. An overview of the measurement setup is shown in figure 2.

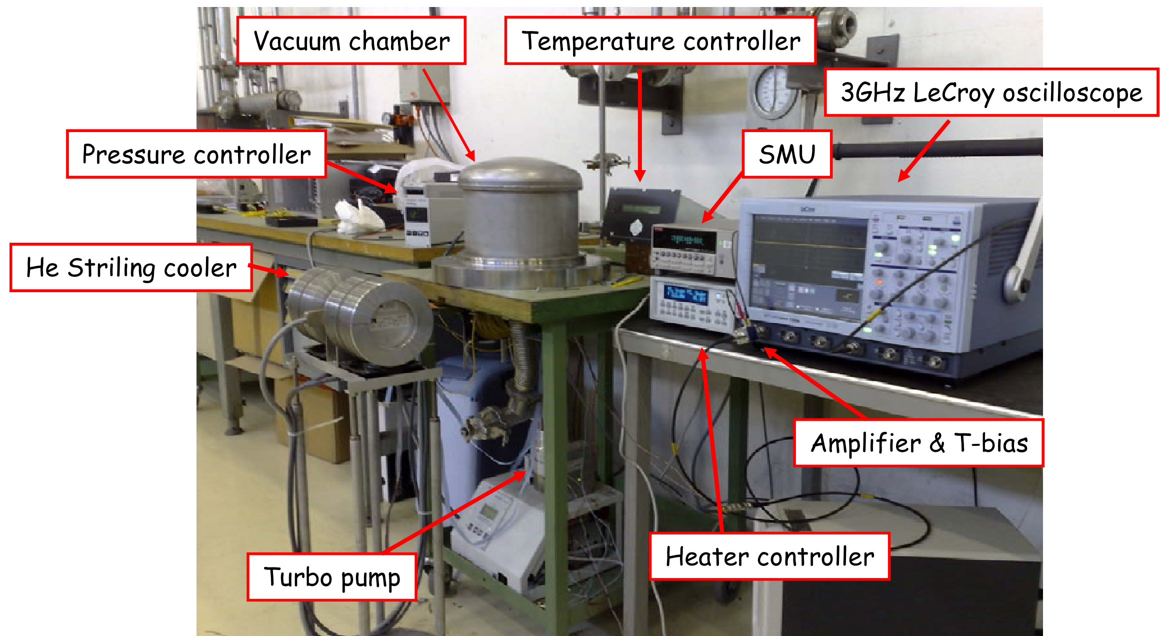

Figure 2. Cryogenic Transient Current Technique (C-TCT) measurement setup.

The biasing circuit, i.e. so called T-bias, has been integrated in our system with a preamplifier. The T-bias providing high DC voltage isolation consists of 30 kΩ resistor and 100 nF capacitors. The signal is amplified between the T-bias and the 50 ΩOHM oscilloscope input by two stage wide bandwidth amplifier having a gain of approximately 600. The amplification stages have been made by ERA-8SM monolithic microwave

integrated circuit (MMIC) analog amplifier chips. A schematic overview of the setup is shown in figure 3.

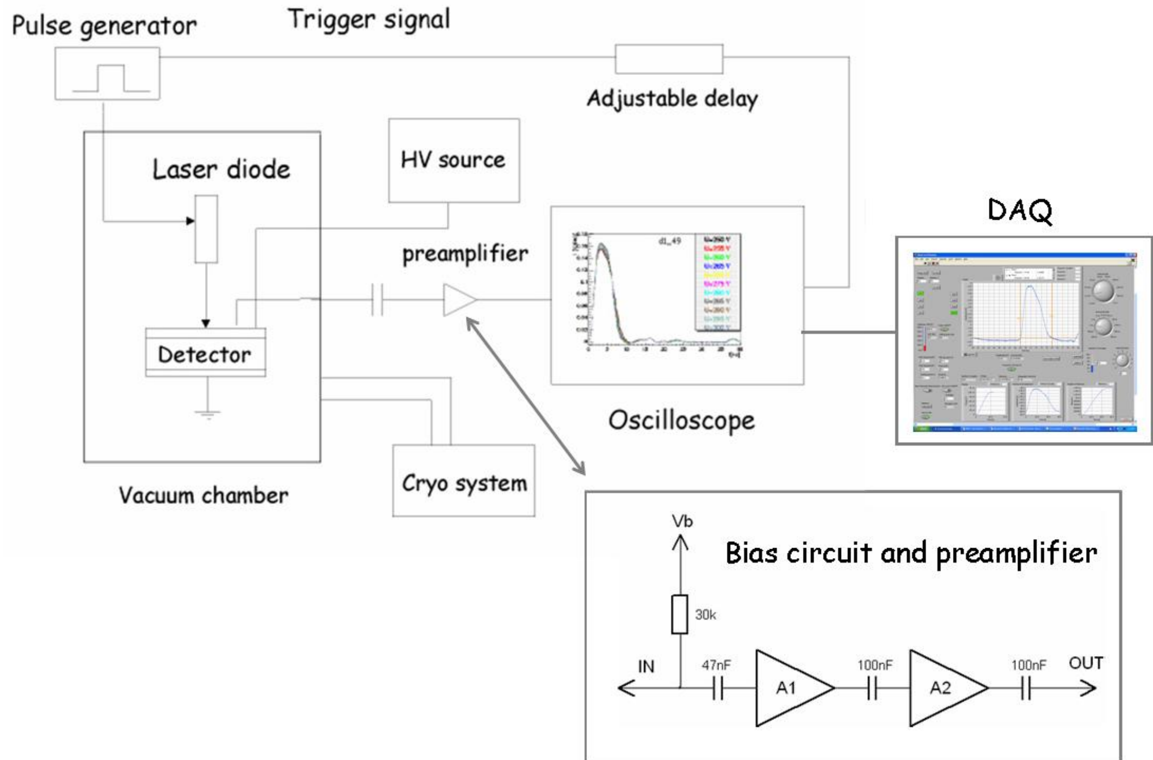

Figure 3. Schematic drawing of the C-TCT measurement setup.

Due to the mechanical design of the copper made cold finger, the diodes could only be illuminated on the front side. The diodes are taped by double sided conductive carbon adhesive tabs on patterned gold plated ceramics. The ceramics have opening in the middle and a gold needle is soldered into the opening. The back contact that provides the high voltage is achieved by inserting the gold needle into a female coaxial connector in the gold finger. The pad contact and guard ring contact of the diodes are wire bonded into the gold metallization of the ceramics. Prior the measurements, the thermal contact between the ceramic and the cold finger are enforced by copper springs. Before the cooling of the cold finger, the vacuum chamber was pumped to 5×10^{-4} mbar pressure. To cool down the cold finger to 60K takes typically one hour. Every measurement took place only after the cold finger temperature saturated within 1 K of the set point. The temperature stabilization takes typically about five minutes. The detectors leakage current is monitored during the temperature stabilization in order to ensure sufficiently small thermal gradient between the sample and the cold finger.

When analyzing the electric field of an irradiated detector, one has to take into consideration that the measured signal is affected by the trapping of the charge carriers into the radiation induced defects. The influence of the trapping can be deducted by applying so called trapping correction method (CCM) [10,11], which is a mathematical manipulation of the measured raw data. The charge correction has been performed by a Matlab program where the user defined input parameters are V_{fd} and the integration time of the recorded TCT signal. The electric field is obtained from the measured TCT signal

by first calculating the trapping time constant. The measured signal is corrected by the trapping constant and by converting the time domain into the distance domain, the electric field is extracted.
The low injection is usually preferred in order to minimize the polarization [9] effects at the cryogenic temperatures. Trapping has no strong temperature dependence and it is inversely proportional to the concentration of trapping centers, while detrapping is exponentially dependent on the temperature. The polarization means rapid decrease of the electric field by free carriers when the whole concentration of traps is filled and remains filled within the signal integration time. An example of a low injection level measurement is shown in figure 4.

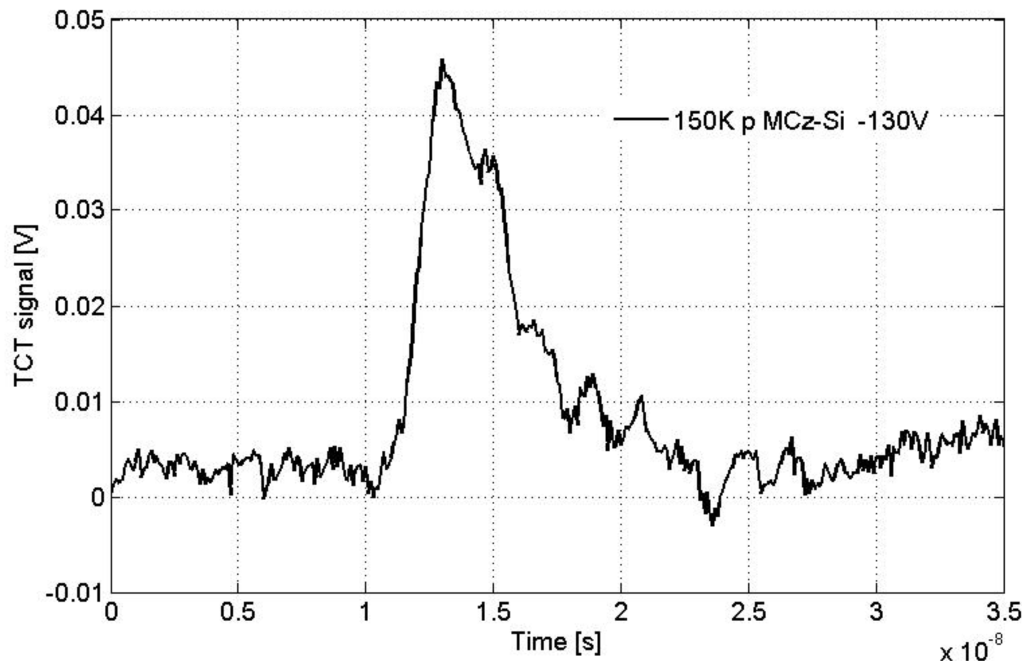

Figure 4. Infrared laser measurement at 150 K for a non-irradiated detector biased over the full depletion. The excitation level in this measurement equals roughly 1 MIP.

The sample in figure 4. is a non-irradiated $n^+/p^-/p^+$ detector, which boron doping has been compensated by the thermal donors (TD) [9]. The V_{fd} of this detector is about -50V. The measurement was done at 150 K and with -130 V bias. During the measurement, the infrared laser was tuned so that the current integrated over 13 ns time window corresponds roughly one MIP, i.e. 24000 electrons in 300 µm thick silicon detector. This is practical minimum level of optical excitation in our system taking into consideration the reasonable signal to noise ratio.

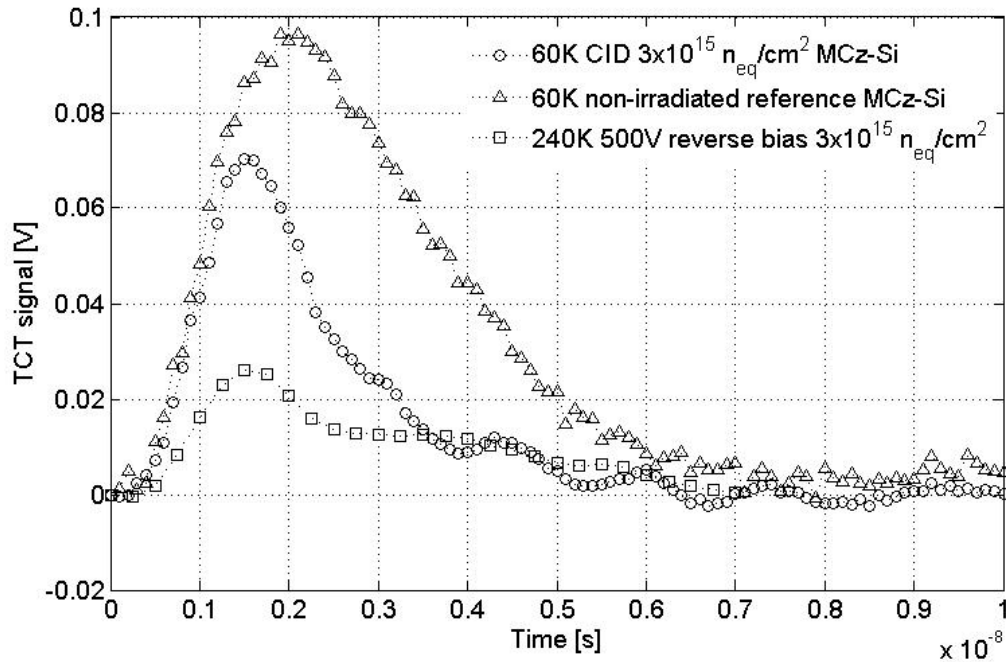

Figure 5. shows the three infrared light responses. The sample has been irradiated by 9 MeV protons [10] to the 1 MeV neutron equivalent fluence of 3×10^{15} cm^{-2} .

The uppermost curve (Δ) is the same detector as in figure 1., but measured at 60K. The second curve (○) is a Current Injected Detector (CID) [12,13,14]. The detector is $p^+/n^-/n^+$ structure made of MCz-Si. It has received 1 MeV neutron equivalent fluence of 3×10^{15} cm^{-2} by 9 MeV protons. At this fluence, its V_{fd} would be order of ~1000 V at temperatures from 0° to -30° C [14]. The bias of the CID detector during the measurement was -500 V. The lowermost curve is the same detector, but measured at 240 K and with 500 V bias, i.e. normal reverse bias operation and moderately low temperature (denoted as PIN). As shown in figure 5., if 100 % CCE is assumed for the reference detector, the CID detector would have about 45 % CCE. In PIN mode, the heavily irradiated detector shows about 27 % CCE, which is expected value according to many studies on this material performed by the CERN RD50 Collaboration [1]. The low CCE is due to the trapping and significant under depletion.

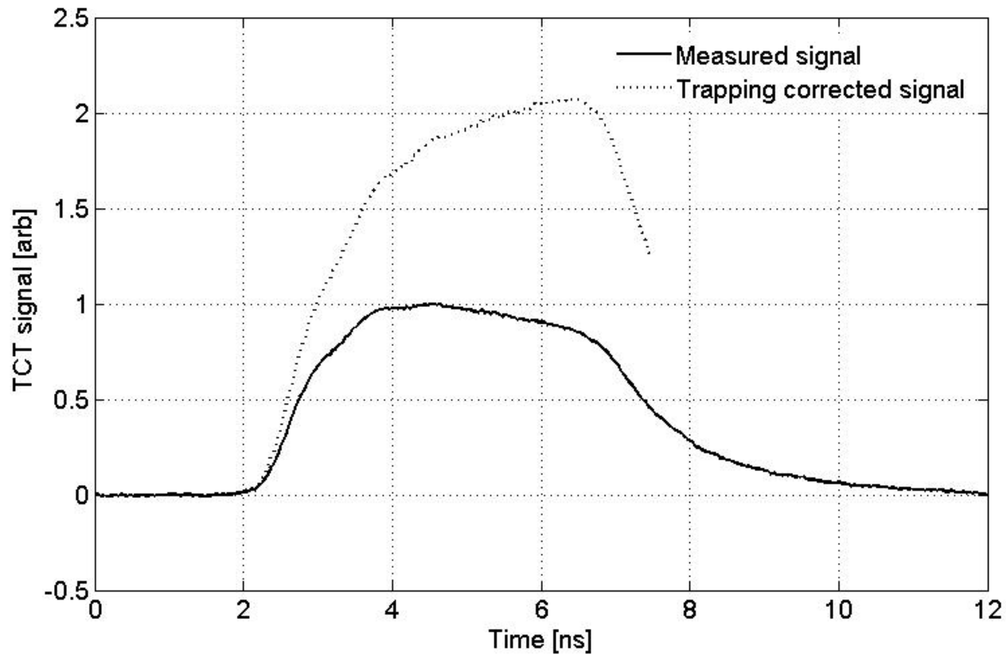

Figure 6. shows TCT measurement made by red laser for $n^+/p^-/p^+$ MCz-Si detector irradiated to the 1 MeV neutron equivalent fluence of 2.5×10^{14} cm^{-2} . The measurement was done at 150 K and with -500 V bias.

The measured signal (solid line) shows clearly decreasing transient with respect of time, thus indicating that the electric field is on the illuminated front side and no SCSI has been taken place. The trapping corrected signal (dashed line), however, shows increasing transient, indicating opposite electric field distribution and SCSI. The extracted hole trapping time constant (τ_h) is 7.9 ns. The SCSI was verified by calculation of the electric field distribution, which is shown in figure 7.

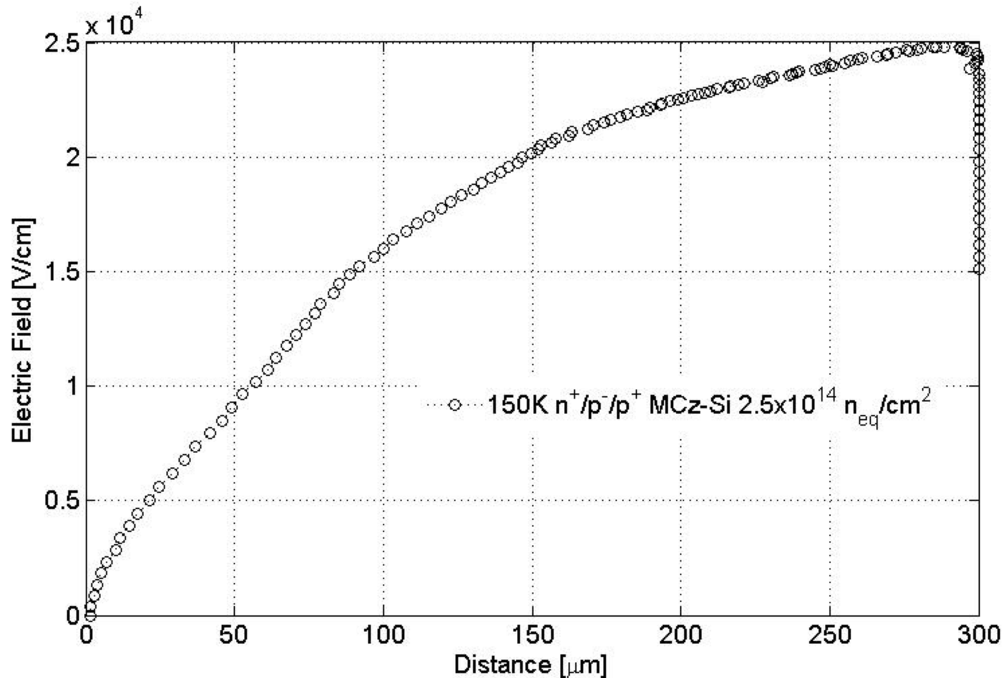

Figure 7. The electric field distribution resolved from the trapping corrected signal.

It can be seen in figure 7. that the electric field has shifted to the back plane of the detector. At the temperatures above 200 K, the electric field and TCT transient, however, unambiguously show that the collecting junction in the same device is on the front side of the detector [15]. Thus, the SCSI is induced by the temperature. At the low temperatures (<200 K) it is apparent that SCSI occurs at certain temperature. This is due that the effective space charge is balanced by the trapping and detrapping. As a consequence, the V_{fd} decreases significantly and the geometrical factor of the CCE is improved.

3. The physics of the Current Injected Detectors (CID)

The method of electric field manipulation is based on the reduction of the negative effective doping concentration (N_{eff}) by injecting holes from the n^+- contact. The effective doping concentration is difference between the ionized acceptor (N_a^-) and donor (N_d^+) concentrations. At the low temperatures the injected holes are captured by radiation induced defects. That results in an accumulation of positive space charge and corresponding reduction of the absolute value of N_{eff} from its initial negative value $-N_{eff0}$. At certain level of injected current the electric field becomes almost uniform meaning that the $|N_{eff}|$ can be reduced close to the zero. When a standard p^+ /i^-/n^+ detector is reverse biased the profit of the injection is related mainly with the reduction of the full depletion voltage. It has been shown that the optimal injected current depends on the detectors operational voltage and the fluence. Therefore the current must be adjusted at any changes of operational parameters.

The mathematical model of the detector with injected current conceders the detector having two electrodes and the silicon bulk in between. The trapping centers produced e.g. by particle radiation are uniformly distributed in the detector bulk. When a bias voltage is applied, the bulk is fully or partially depleted depending on the electric field distribution defined by the density of charged donors and acceptors. To compensate the negative $N_{eff\ 0}$ and overcome the collapse of electric field under irradiation the injection of hole current is applied through the n^+ contact. The injected holes are trapped by deep levels resulting in reduced negative effective concentration and more uniform electric field distribution. The Poisson equation, Ohm's law and rate equation define the steady state electric field distribution in semiconductor bulk. Thus, the CID approach can be formulated mathematically by set of 3 equations.

$$\frac{dE}{dx} = \frac{q_o}{\varepsilon\varepsilon_o}\left(p_t + N_{eff0}\right) \qquad (1)$$

$$\frac{dp_t}{dt} = -\frac{p}{\tau_t} + \frac{p_t}{\tau_d} = 0 \qquad (2)$$

$$p = \frac{j}{q_o \mathrm{v}_{dr}} \qquad (3),$$

where τ_t and τ_d are trapping and detrapping time constants given by

$$\tau_t = \left[\sigma \mathrm{v}_{th}\left(N_t - p_t\right)\right]^{-1} \qquad (4)$$

$$\tau_d = \left[\sigma \mathrm{v}_{th} N_\mathrm{v} \cdot \exp\left(-\frac{E_t}{kT}\right)\right]^{-1} \qquad (5)$$

In equations (1)-(5) the p is the free hole concentration, p_t is the concentration of holes captured by deep levels with a concentration N_t, q_o is the value of the elementary charge and ε and ε_0 are, respectively, the permittivity of silicon and the vacuum, σ is the hole capture cross section, v_{th} is the hole thermal velocity, N_v is the effective density of states in the valence band, E_t is the activation energy of the deep level, k is the Boltzmann constant and T is the absolute temperature, v_{dr} is the hole drift velocity. The boundary conditions can be set in form $E|_{x=0} = E_o$.

Solution of the equations set gives the relationship between the electric field E and the x coordinate in the following implicit form

$$x = \frac{1}{P}\left[\frac{Bj + q_o \mathrm{v}_s}{R}\left(E - E_o\right) + \frac{Bj\left(CR - 1\right) - q_o \mathrm{v}_s}{R^2} \cdot \ln\left(\frac{RE + 1}{RE_o + 1}\right)\right] \quad (6)$$

Where the parameters are:

$$A = -q_o/\varepsilon\varepsilon_0;\ B = \sigma \mathrm{v}_{\mathrm{th}} \tau_d;\ C = \mathrm{v}_s/\mu_o \qquad (7)$$

$$P = ABC\,j\left(N_{eff0} + N_t\right)$$
$$R = \frac{1}{C}\left[1 + \frac{q_o \mathrm{v}_s N_t}{B\,j\left(N_{eff0} + N_t\right)}\right] \qquad (8)$$

Numerical calculations of the electric field distribution were carried out for detectors irradiated by a neutron fluence Φ_n in the range 1.4×10^{14} cm^{-2}. For a comparison with the experimental data, most results were obtained for the conditions corresponding: $\Phi_n = 1.4\times\cdot10^{14}$ cm^{-2} and operational bias $V = 210$ V. The injection of hole current density was in the range of 100 pA/cm^2 to 20 nA/cm^2. It was assumed that the injected holes were captured by radiation induced C_i-O_i defect complexes, which act as hole traps with parameters: $E_t = E_\mathrm{v} + 0.37$ eV; $\sigma_h = 3\cdot10^{-15}$ cm^2 [3], [13]. The space charge concentration after irradiation, N_{eff0} was evaluated from the Φ_n and assumed to be -1.05×10^{13} cm^{-3} at $\Phi_n = 1.4\times10^{14}$ cm^{-2}.

The calculated dependencies of the electric field distribution in a detector irradiated by $\Phi_n = 1.4\times10^{14}$ cm^{-2} on the hole injection current density at $T = 140$ K are presented in Fig. 8. The initial $E(x)$ at $j = 0$ and $T = 140$ K is a standard linear dependence on x, with a maximum value of $E_o \approx 26$ kV/cm at the n^+-contact due to the negative value of N_{eff0}. The depth W of the SCR under these conditions is about 162 µm, i.e. less than the geometrical detector thickness $d = 280$ µm. Injection of a hole current of $j = 1$ nA/cm^2 modifies the electric field only slightly. At $j = 8$ nA/cm^2, however, the SCR extends up to the detector p^+-contact, i.e. the detector becomes fully depleted. Nevertheless, two regions with a different $E(x)$ profile are evinced at this current: a region with a linearly decreasing $E(x)$ starting from the n^+-contact, and grading into a region with a low, practically constant electric field adjacent to the p^+-contact. At $j = j_{opt}$ (~16 nA/cm^2) the electric field distribution is close to a uniform one. The calculation for $j > j_{opt}$ shows that excess hole trapping results in an essential modification of the $E(x)$ profile in which the maximum electric field is shifted to the p^+-contact due to the dominating positive space charge.

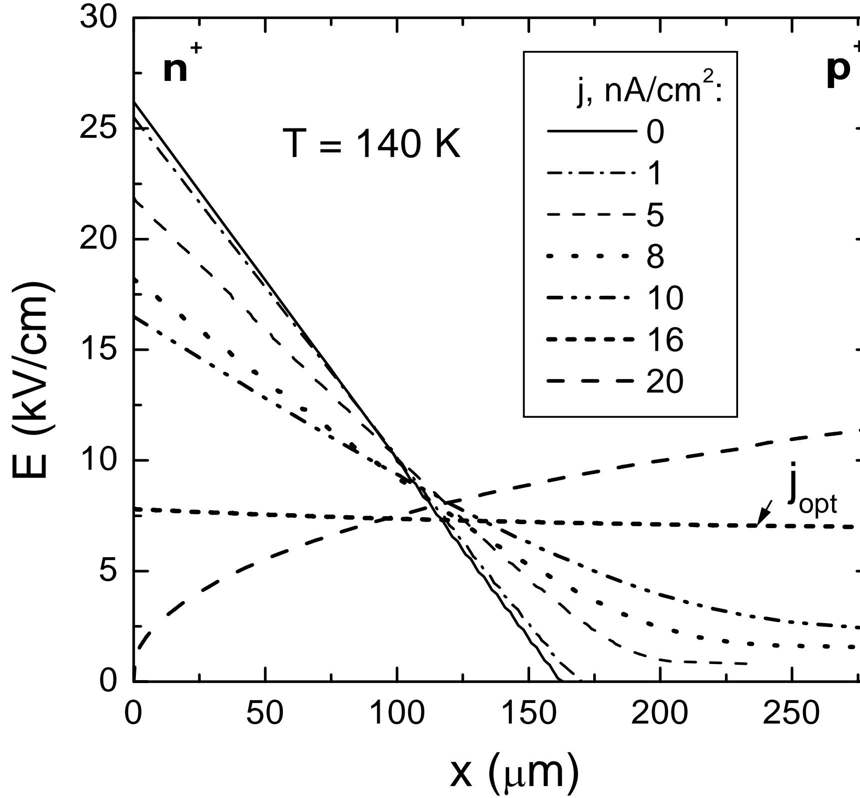

Figure. 8: Dependence of the electric field distribution on the hole injection current density in silicon detector irradiated by neutrons $\Phi_n = 1.4\cdot\times10^{14}$ cm^{-2}; $V = 210$ V.

The full range of the appropriate injection current (operational range) covers the currents corresponding to detector full depletion. For instance, for the detector considered here (irradiated by $\Phi_n = 1.4\times\cdot10^{14}$ cm^{-2} and operating at $T = 140$ K), this range is between $j \approx 8$-20 nA/cm^2. 8 nA/cm^2 reduces N_{eff} sufficiently to achieve full depletion under the given bias (210 V). With $j \approx 20$ nA/cm^2 injection the electric field at the n$^+$-contact is close to zero. Significant non-linearity of $E(x)$ is predicted only at the limits of the injection current range. Thus, for a detector irradiated by a fluence of 1.4×10^{14} cm^{-2}, the range of j from 8 to 16 nA/cm^2 can be considered as optimal for full depletion of a detector operating at $T = 140$ K.

Obviously, the operational current range and the electric field distribution is different for different bias voltage, temperature and irradiation fluence.

The main problem for application of this approach is it the technical realization. Generation of hole injection needs the transparent n$^+$ contact and the controlled uniform intensity of light. Because to the detectors are placed in the area with hard radiation environment the light sources must be stable and radiation hard as well. This disadvantage reduces the area of application for CID detectors operated at reverse bias. However as a tool for defect characterization it can be successfully used because the electric field is sensitive to the deep level parameters and temperature.

3.1 CID with self stabilized current injection

As shown in figure 8 the increase of injected current leads to reduction of the electric field at the injecting contact. At the current of 20 nA/cm^2 the electric field at x=0 falls down to zero. If the electron-hole pair generation at the surface that injects charge into the bulk is further increased, it does not increase the current. This is because of full screening of free carriers. In other words, the electric field prevents the injection of electrons into the detector volume.

The theory of current flow in insulators defines this phenomenon as a space charge limited current effect. The condition for the space charge limited current is a zero electric field at the injection surface. This condition together with equations (1) – (3) defines the physical properties of the detector:

1) The electric field is proportional to square root of the distance from the injection contact ($E(x) \sim \sqrt{x}$)
2) The current is proportional to the second power of voltage ($\sim V^2$)
3) The concentration of deep traps determines the amount of current ($J \sim 1/N_{dl}$).

There are two ways for this mode realization. First, the above discussed current generation by any ionizing radiation like light or short range particles illuminating the contact. The intensity should be high enough to create the plasma of free carriers at the contact. Second, current injection from p-n junction as an emitter of electrons or holes.

The first approach leads to technical difficulties as it was mentioned above and could not be realized in the frame of existing concepts for the complicate tracker systems in high energy physics experiments. The second approach is more practical because the pn-junction emitter is a vital part of every detector. Then only the optimal temperature and the bias remain parameters to be optimized.

The CID has a symmetric structure with two identical junctions on the detector sides. At any polarity one of the junctions will be biased in forward direction and the other in reverse. The contacts are highly doped p$^+$ layers and therefore forward biased contact will inject holes and the reverse biased will collect them. The mathematical model, presented in previous chapter, fits well to the solved equations with the boundary condition on the injecting contact $E(x)=0$.

The experimental I-V characteristic of CID with symmetric p+-n-p+ structure is shown in Fig 9.

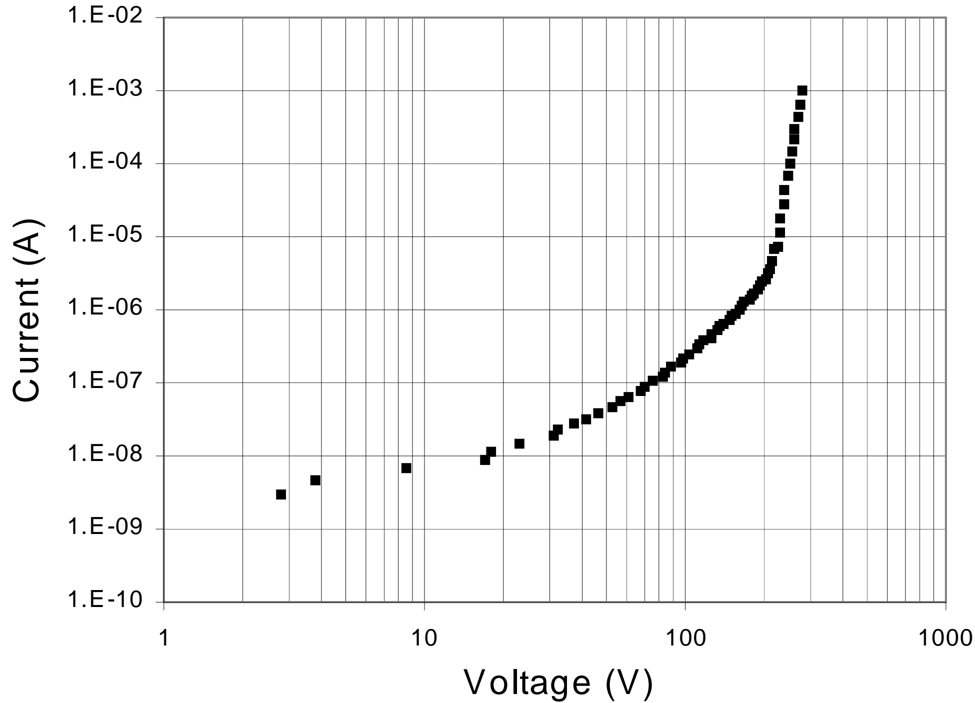

Figure. 9. Experimental I-V curve for p^+-n-p^+ detector irradiated by a fluence of 1×10^{15} n_{eq}/cm^2 at a temperature of 200 K.

In figure x. there are three parts distinguished. First at low bias (3-20V), there is linear current voltage dependence. This could be nominated as Ohmic part of the IV curve. First part is followed by quadratic current voltage relationship (20-200V). This is characteristic of the space charge limited current effect. Third section of the IV curve can be seen after 200 volts. The sharp rise is a specific feature of the space charge limited currents. It related to the saturation of the deep traps with trapped curriers. In this case the injection can not be limited anymore.

It has been shown that heavily irradiated silicon detectors can operate at both polarities of the bias at the cryogenic temperature [12]. This observation was investigated in the frame of developing CID concept and the I-V curves of the forward biased PIN detectors are shown in figure 10. Comparisons of the data in figures 10 and 11, shows that the main features of space charge limited current are well observed for PIN detector. The slope of 2 and the sharp rise are specific for both structures. The I-V curves fit (solid lines) by the above described model allows to define parameters for the effective deep level responsible for the space charge limited current effect.

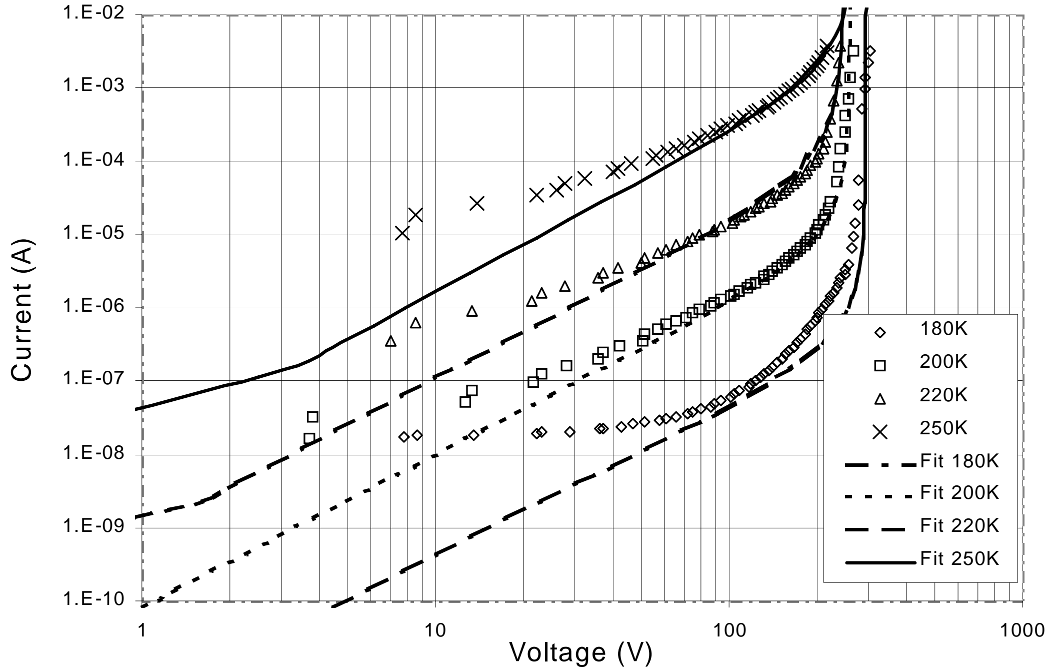

Figure. 10. Experimental and simulated I-V dependences of p^+-n-n^+ CID irradiated by a fluence of $1\cdot10^{15}$ n_{eq}/cm^2 operated at different temperatures.

It was discovered that the appropriate effective trap is a donor like level with activation energy of E_t - E_v = 0.478 eV. The capture cross-section for electrons and holes was set of 1×10^{-15} cm^2 and N_t in the range 3.8 – 4.2×10^{12} cm^{-3}. With these parameters the set of I-V curves measured at different temperatures was fitted. The value of N_t was slightly adjusted to fit mainly the sharply rising part of the I-V characteristics. The parameter of the defined effective trapping center corresponds to the parameters of the mid-gap deep donor that was identified earlier as one of the two mid-gap levels responsible for the operational characteristics of heavily irradiated silicon detectors [16], [17].

In order to test the model, the fitted defect parameters were used to calculate I-V curves and compared with experimental data of CID detectors irradiated with different fluences. The result is shown in fig 11.

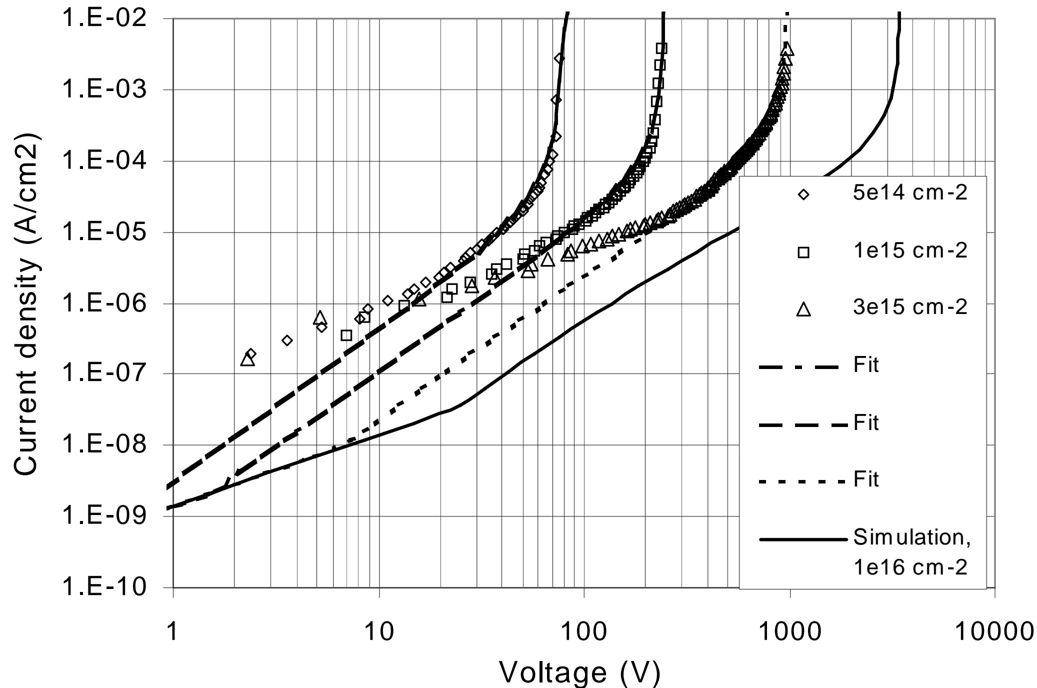

Fig. 11. Experimental and simulated normalized I-V curves of CID irradiated by different fluences and operated at 220 K.

It can be seen in figure x. that within almost an order of magnitude of irradiation fluence, the fitted lines correlate with the major trend of the experimental I-V curves. Only in the voltage region less than 100V discrepancies are observed. The reasons for that is the surface leakage current and possible injection of electrons from the backside n^+-n junction of the p^+ - n^- n^+ structure. However, at high value of the injected current the hole injection dominates and the quadratic law is apparent. The curve for 1×10^{16} n_{eq}/cm^2 is a prediction based on the same defect parameters with the proportionally increased the trapping centers concentration.

The important aspects in scope of practical applications of CID detectors are the range of the operation voltage, temperature and the amount of the forward current. The most influential effect of the irradiation fluence in the CID detector I-V curve is the increase of the threshold voltage V_{th} at which the current starts to increase rapidly. This trend is well demonstrated in Fig. x, where V_{th} is plotted as a function of neutron fluence.

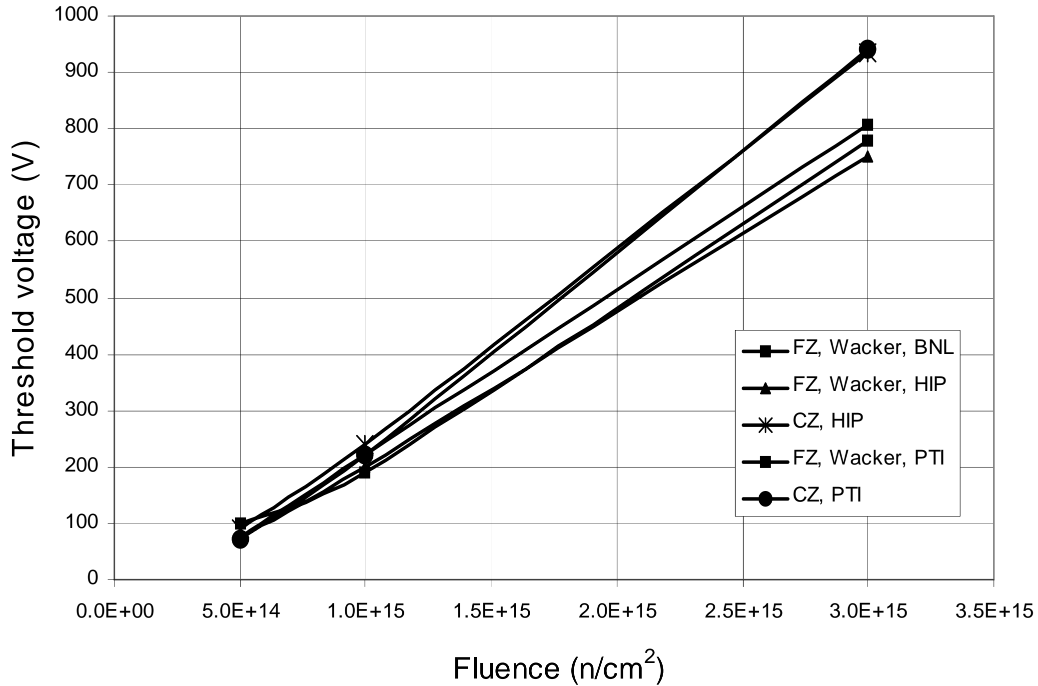

Fig. 12. Dependence of threshold voltage on irradiation fluence for current injected detectors processed from different types of silicon and processed at different facilities.

The threshold voltage increases linearly with fluence with $dV_{th}/d\Phi = 2\times10^{-13}$ Vcm^2. For the expected maximal fluence of 3×10^{15} cm^{-2} for S-LHC it is near 1000 V, far above the operational voltage of 300-500 V used in the ATLAS and CMS inner tracker detectors now being constructed for the LHC.

The figure 13 illustrates the unique feature of CID detectors – the decrease of the detector current with increase of the irradiation fluence. The current as a function of fluence at constant operational voltage 200V is presented in figure 13.

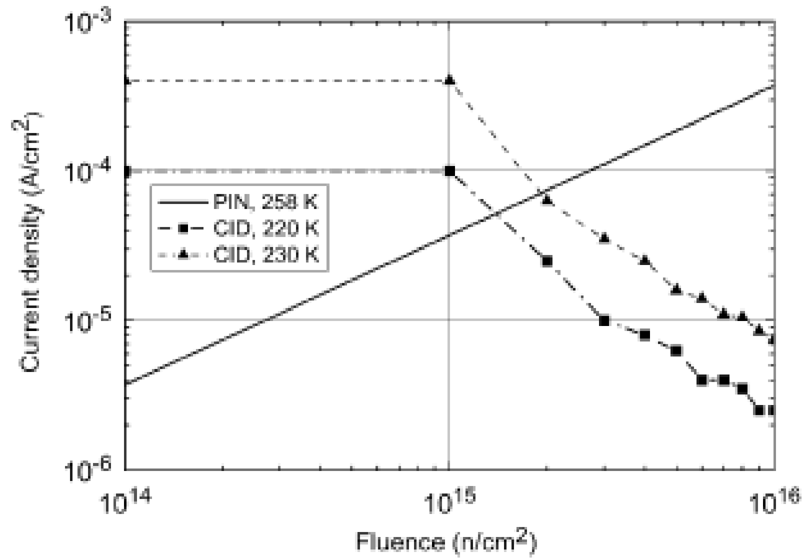

Figure 13 The current as a function of fluence at constant operational voltage 200V. The deep level introduction rate is 4×10^{12} cm^{-3} at 1×10^{15} n_{eq}/cm^2 fluence, $V_{pin} > V_{fd}$

The current is progressively decreasing with fluence as it is expected from the CID physics. The rate of the current decreases is $F^{-1.5}$. Obviously, the current is lower for the operation at lower temperature due to reduction of the emission rate of the trapping centers.

3.2 Charge Collection Efficiency (CCE) and noise of CID detectors

The CCE data shown in this chapter has been independently measured with two Transient Current Technique (TCT) measurement units at the Ioffe PTI [13] and at CERN [18]. The measurements have been performed by using 1060nm infrared lasers that generate homogenously electron hole pairs through the entire thickness of the silicon bulk and therefore simulate the excitation caused minimum ionising particles (MIP) [9]. 5-10% error margins could be assumed for measurements of this kind. The collected charge as function of bias voltage Q(V) is shown in figure 14. We denote PIN as the same sample, but biased with opposite polarity.

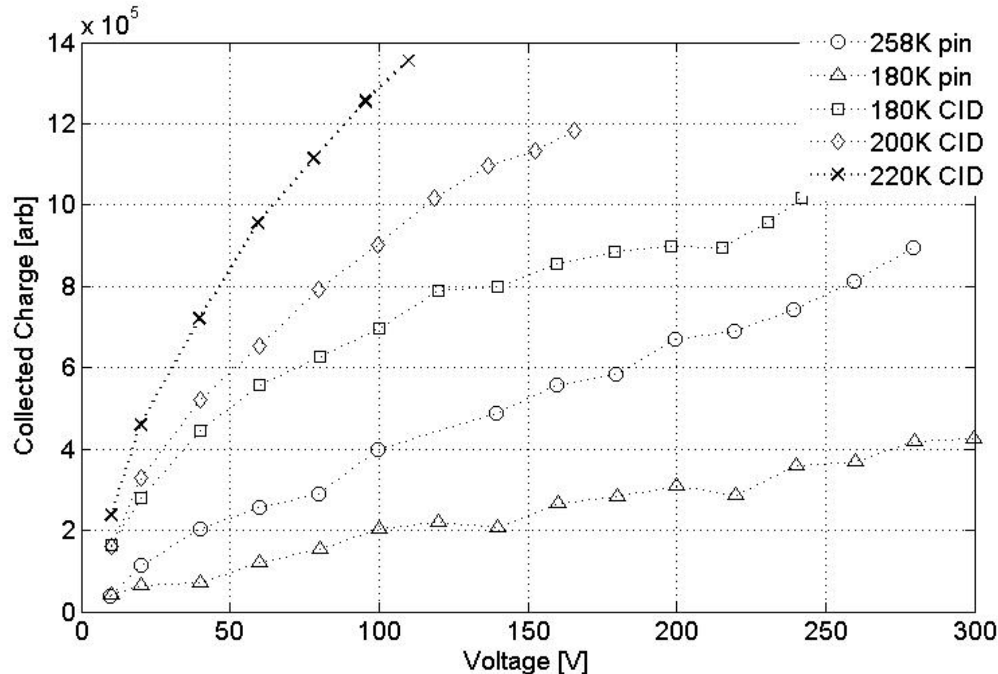

Figure 14. Collected charge as function of voltage at different temperatures. The sample is MCz-Si diode irradiated by neutrons to the fluence of 1×10^{15} cm^{-2}. The curves Δ and ○ correspond normal detector operation with reverse bias. The curves □, ◊ and × are for CID operation.

The sample used in this measurement at the PTI is n-type Magnetic Czochralski silicon (MCz-Si) diode irradiated with neutron to the fluence 1×10^{15} cm^{-2} and having area of 0.25 cm^2. At this fluence, the full depletion would require about 1000 V reverse bias [19]. The charge was measured after one minute stabilization after every bias step. The charge integration is done over a collection time of 15 ns. The charge is presented in arbitrary units, which are the same for CID and for PIN detector. The shape of the charge rising with bias for PIN detector is close to linear that follows from the dependence of the geometrical factor for MIP particles (Width of the depleted region W / detector thickness d)^2 and the space charge propagation rate on the applied bias of $W^2 \propto V$. This indicates that PIN up to 300 V is not fully depleted while the CID is "depleted" at any bias. Contradictory to the normal detector operation, there is no saturation of the collected charge after "full depletion" because the electric field increases with the increasing forward bias. The shape of the Q(V) is not linear. This is due to drift velocity saturation in electric field. Consequently the CID's provide signal up to 3.5 times higher compared with PIN detectors at the same voltage. Even at the bias 300 V the PIN detector shows lower signal than CID at 100 V. This illustrates advantage, which CID provides for the experiments – possibility to collect charge effectively even at the relatively low bias voltage of 100-200 V.

Figure 15. shows the infrared light responses of three detectors.

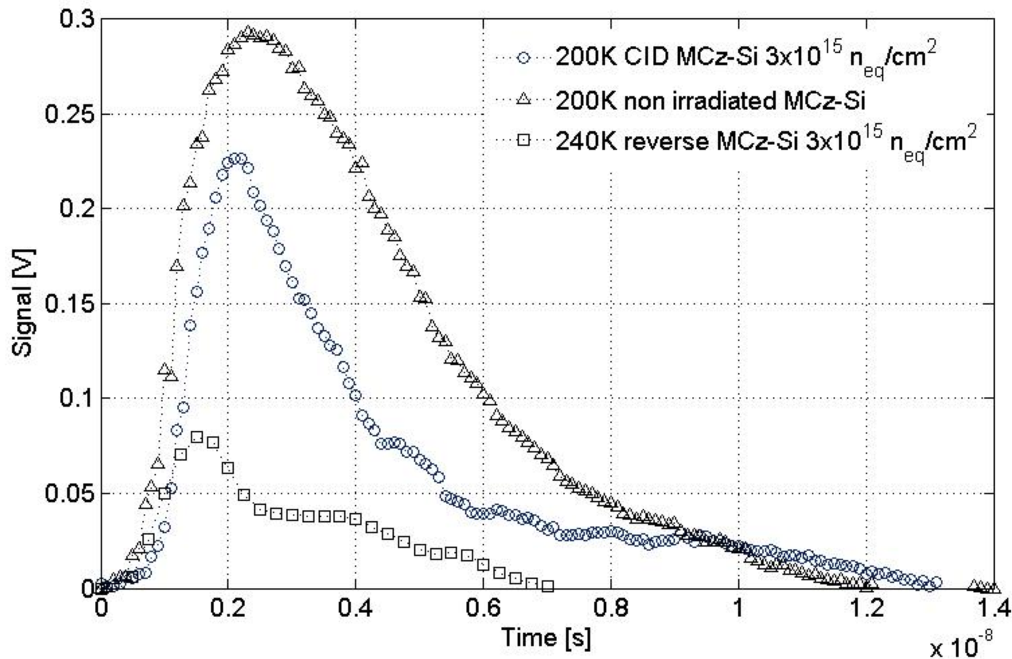

Figure 15. Infrared laser signals of reference non-irradiated (Δ) MCz-Si detector, CID at 200K (○) and same detector in normal operation at 240K (□). The injection level during the measurements was about 10 MIPs.

The CCE measurement was performed by the CERN RD39 Collaboration. The sample has been irradiated by 9 MeV protons [20] to the 1 MeV neutron equivalent fluence 3×10^{15} cm^{-2} . For reference and calibration purposes, a non-irradiated MCz-Si diode was measured simultaneously with exactly same experimental arrangement. The V_{fd} of the p-type thermal donor (TD) compensated MCz-Si reference detector is about 50 V [21]. During the measurement, the reference was biased to 200V, CID and the same detector in PIN mode to 500 V. As shown in figure 3., if 100% CCE is assumed for the reference detector, the CID detector would perform about 65% CCE. The CID detector was also measured as PIN at 240 K, which has been proposed to be operational temperature of future upgrades of LHC experiments. In PIN mode, the heavily irradiated detector shows about 27% CCE, which is expected value according to many studies on this material performed by the CERN RD50 Collaboration [1]. The low CCE is due to the trapping and significant under depletion. It should be emphasized that the forward current in CID detector at 500V is 1.6 μA, which is less than under reverse bias at 500V and 240K.

As pointed out in previous chapter, the current progressively decreases with fluence (F). This is expected from the CID physics and verified by several independent measurements [14,18]. The rate of the current decreases is $F^{-1.5}$. Obviously, the current is lower for the operation at lower temperature due to reduction of the emission rate of the trapping centers. A simulation of the noise in silicon strip detector is shown in figure 16.

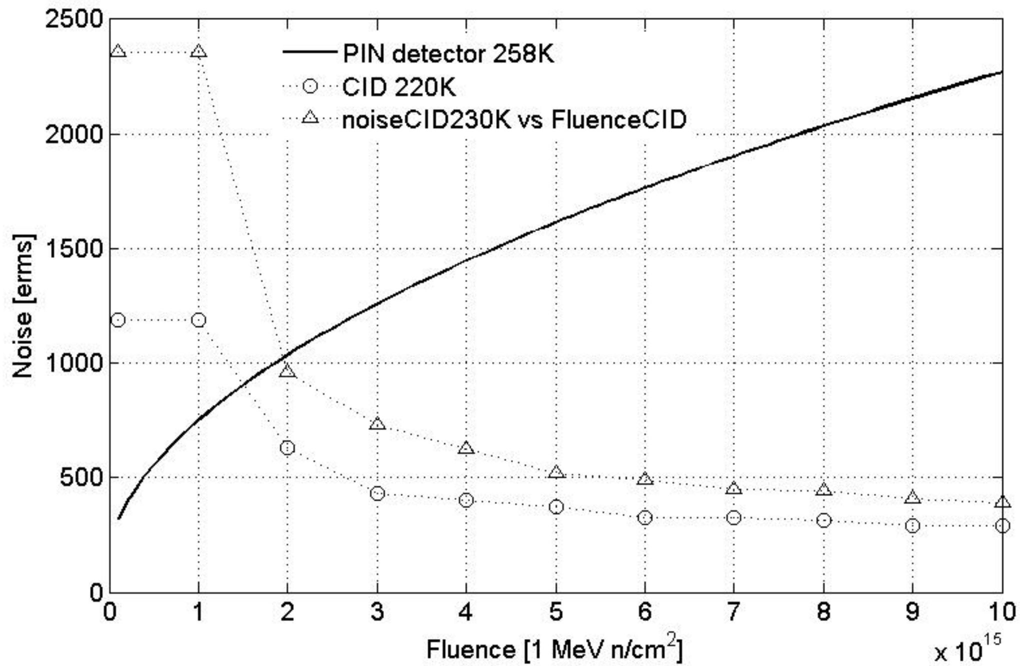

Figure 16. Simulation of noise performance of CID detector versus normal detector operation.

The simulation has been made according to the strip detector design of CERN ATLAS experiment: pitch 80 µm, strip length 6 cm and read-out shaping time 25 ns , PIN is biased to the full depletion and the temperature is 258 K. The bias for CID is 200V. As it can be seen, at fluence 2×10^{15} n_{eq}/cm^2 the CID noise becomes lower than in PIN detector.

In order to verify the CID operation, it is necessary to test devices irradiated with different particles. Set of MCz-Si detectors were irradiated by 24 GeV/c protons at CERN Irrad1 facility. The maximum proton fluence in this irradiation campaign was 1.6×10^{16} p/cm^2 , which equals irradiation that innermost pixels sensors will receive after ten years operation of Super-LHC trackers. Figure 17 shows IR laser response of heavily 24 GeV/c irradiated detectors.

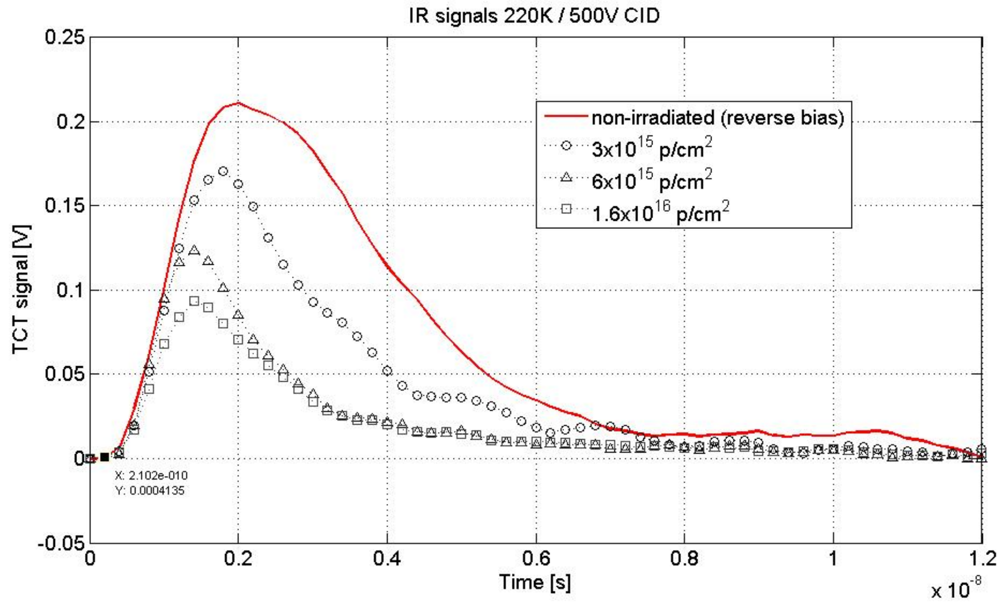

Figure 17. IR signals of high energy proton irradiated CID detectors with respect of non-irradiated reverse biased reference detectors.

The measurements shown in figure x are performed at 220K and at 500V constant forward bias. In order to compare CID detectors to normal detector operation, the same devices we measured also under 500V reverse bias and at 220K conditions. The figure 18 shows the IR signals recorded from 1.6×10^{16} p/cm^2 irradiated sample.

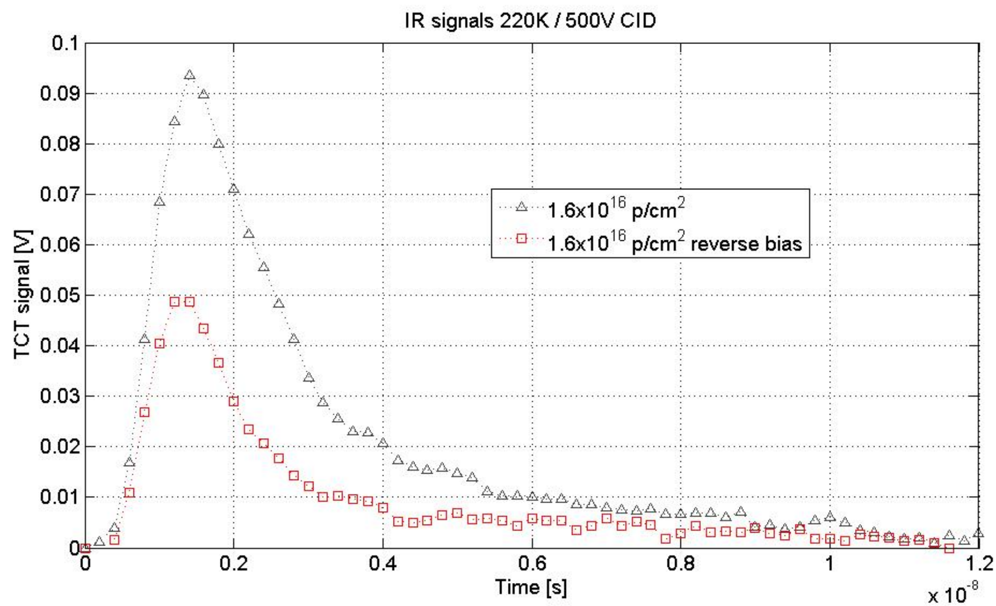

Figure 18. 1.6×10^{16} p/cm^2 irradiated detector measured in CID (Δ) and in reverse bias (□).

One can qualitatively see in figure x, that the collected charge is about two times higher in CID operation than under reverse bias. Figure x shows collected charge as function of irradiation fluence for low and high energy proton irradiated MCz-Si detectors.

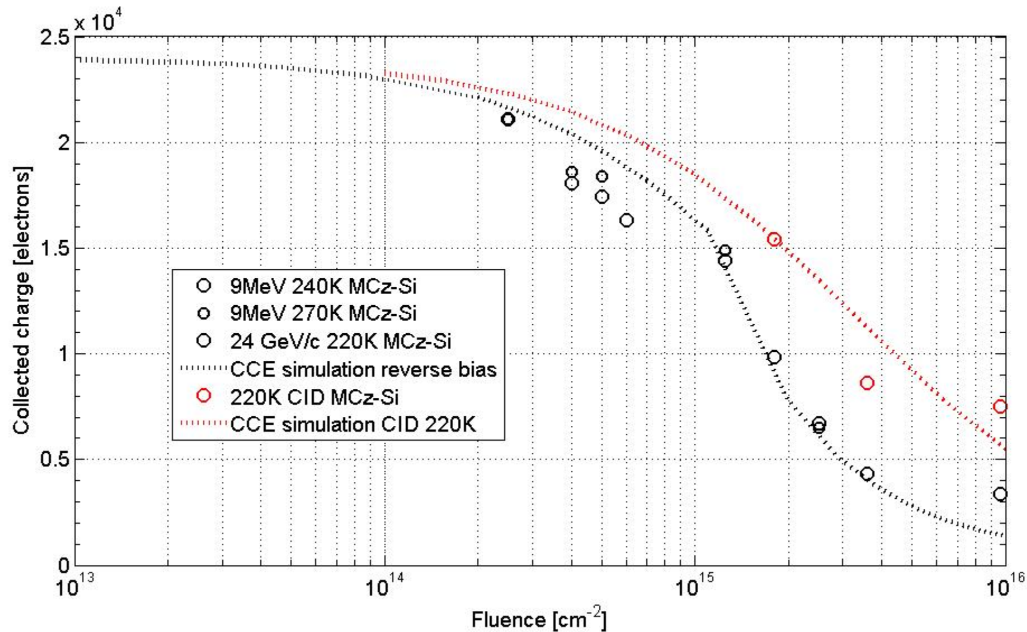

Figure 19. Collected charge vs fluence of 9 MeV and 24 GeV/c proton irradiated MCz-Si detectors. The red ○ symbols denote CID data points. The data points below 1×10^{15} n_{eq}/cm^2 have been measured at 240K and 270K, while data points above 1×10^{15} n_{eq}/cm^2 at 220K. The dashed lines are CCE simulations.

The CCE simulation shown in figure x takes account the evolution of V_{fd} and trapping. The β factor in this simulation is 0.01 cm^{-1} and the trapping is assumed to be linear, i.e. τ_{trap} at 1×10^{15} n_{eq}/cm^2 is 1ns and at 1×10^{16} n_{eq}/cm^2 is 0.1ns. The CID simulation assumes square root distance depended electric field predicted by the theory described is previous chapter.

3.3 Summary of Charge Injected detectors.

The major advantage of current injection in the detectors bulk is the maintenance of the electric field through the entire volume regardless of irradiation fluence. Despite of trapping effects, this result in about two times higher CCE than in detectors operated in standard reverse bias mode. The elevated CCE is achieved in the temperature range of 220-240K.

The most promising construction of CID is a symmetric structure, which ensures the current injection from only one of the contacts. Because the acceptor like levels are dominating in the irradiated silicon, the p+-i-p+ detector structure, which provides at any bias is hole injection, is most promising candidate for optimal CID operation. It is possible, however, operate normal detector structures as CID.

An important step in the CID development is the understanding of the space charge limited current phenomenon for the injected current stabilization. The CID with self stabilized current injection exhibits all major behaviors of the space charge limited

current that in turn gives a proof of the concept and allows the CID engineering and optimization of their operational mode. With the defined microscopic parameters of the effective trapping center, the CID model predicts a unique detector behavior: with the fluence increase the CID operational bias range becomes wider and the leakage current decreases. Consequently, the noise performance of CID is improving with progressive irradiation. Additionally, the CID operates at any bias like a full depleted detector, thus the geometrical factor of the amplitude deficit is diminished. As a result, the signal amplitude up to several times higher than for the conventional PIN detector even for the significantly low bias voltage.

It was observed that the regular PIN detectors can operate at current injection mode with dominating injection from one of the contact. This observation need to be physically explained. However for application it gives possibility to exploit PIN detectors in forward bias mode as CID.

The CID is potentially very cost effective solution for S-LHC detectors, because the processing technology as well as silicon properties does not influence the CID performance.

References

[1] M. Bruzzi et al.; Radiation-Hard Semiconductor Detectors for Super LHC; Nucl. Instr. and Meth. A 541 (2005) 189-201.
[2] E. Verbitskaya et al, Nucl. Instr. and Meth. **A 514** (2000) 47.
[3] E. Gatti, G. Padovini, and V. Radeka, Nucl. Instr. and Meth. **A 193** (1982) 651.
[4] V. Radeka, Ann. Rev. Nucl. Part. Sci., 38 (1988) 217.
[5] S. Parker, C. Kenney, and J. Segal, "3D—A proposed new architecture for solid-state radiation detectors," Nucl. Instr. and Meth., vol. A395, Aug. (1997) 328–343
[6] Z. Li and H.W. Kraner, "Modeling and Simulation of Charge Collection Properties for Neutron Irradiated Silicon Detectors", Nucl. Phys. B (Proc. Suppl.) 32 (1993) 398-409)
[7] H.W. Kraner et al., Nucl. Instr. and Meth. A326 (1993) 350-356M. Bruzzi et al.; Nucl. Instr. and Meth. **A 541** (2005) 189-201.
[8] H.W. Kraner et al., Nucl. Instr. and Meth. A326 (1993) 350-356
[9] B. Dezillie et al., Nucl. Instr. and Meth. A452 (2000) 440.
[10] T. J. Brodbeck, et al., Nucl. Instr. and Meth A455 (2000) 645.
[11] G. Kramberger, et al., Nucl. Instr. and Meth A476 (2002) 645.
[12] V. Eremin et al., IEEE NSS Conference Record, 2004 IEEE Vol. 3,16-22 (2004), 2003–2006.
[13] V. Eremin et al., Nucl. Instr. and Meth **A583** (2007) 91.
[14] V. Eremin et al., Nucl. Instr. and Meth **A81** (2007) 356.
[15] J. Härkönen et al., Nucl. Instr. and Meth **A583** (2007) 71.
[16] V. Eremin, Nucl. Instr. and Meth **A372** (1996) 388-398.
[17] V. Eremin et al., Nucl. Instr. And Meth, **A372** (1996) 188.
[18] RD39 Status Report CERN-LHCC-2006-03
[19] E. Tuovinen et al., Nucl. Instr. and Meth. A 568 (2006) 83-88.
[20] S.Väyrynen et al., Nucl. Instr. and Meth **A572** (2007) 978.
[21] J. Härkönen et al., Nucl. Instr. and Meth **A599** (2007) 648.

Workplan 2007-2008

Schedule for the projects of RD39 in 2007 and 2008

Year	2007	2008
Task	Qtr1 Qtr2 Qtr3 Qtr4	Qtr1 Qtr2 Qtr3 Qtr4
Characterization of CID operation of irradiated strip detectors with read-out electronics	XXX	XXXXXXXXX
H-bar like installation of small Peltier elements in the back side of sensor to cool the detector down to -50 °C		XXXXXXX
CID measurements on segmented (strip) Si detectors At 220-250K		XXXXXXXX
Beam test on CID segmented (strip) Si detectors		XXXXXXXXXXX
Implementation of CID concept on edgeless detectors		XXXXXXXXXXXXXX
More detailed CID modeling	XX	XXXXXXXXXXXXXX
Simulations of injection and E field at cryogenic temperatures	XX	XXXXXXXXXXXXXX
Modeling of trapping at CID conditions at low temperatures	XX	XXXXXXXXXXXXXX

Resources

Resources of the 15 institutes in RD39, planned for the projects of RD39 for 2008. For institutes involved also directly in the experiments, the resources for the construction of the final detectors are not included in the figures given for the budget and for the FTE manpower.

Institute	Authors	Device Physics	Basic Research	Cryogenic Modules	RD39 Budget (CHF/year)	FTE In RD39
U. Northeastern	5	x	x		1000	0.50
BNL	2	x	x	x	20000	1.00
CERN	2	x	x		2000	1.00
U. Florence	4	x	x		4000	1.00
U. Geneva	1	x		x	1000	0.15
U. Glasgow	2	x	x		2000	0.50
HIP Helsinki	4	x	x		20000	1.00
U. Helsinki	4	x	x		10000	2
U. Karlsruhe	7	x	x		5000	2.00
U. Louvain	3	x		x	20000	1.00
JSI Ljubljana	4	x	x		2000	0.50
U. Naples	3			x	2000	0.50
Ioffe PTI	3	x	x	x	10000	1.50
U. Turku	3	x	x		5000	0.60
U. Vilnius	7	x	x		10000	2.0
Total	54	14	12	5	109000	14.25